PORE PRESSURE RISE IN CEMENT MORTAR WALLS SUBJECTED TO FIRE

Kazunori HARADA
Department of Architecture, Kyoto University,
Sakyo-Ku, Yoshida-Hon-Machi, Kyoto, 606-01, Japan

Toshio TERAI
Department of Architecture, Kinki University,
Takayaumenobe 1, Higashihiroshima, Hiroshima, 729-17, Japan

ABSTRACT

Numerical analyses were carried out to investigate the pore pressure rise in cement mortar walls during fire. The analytical model takes into account of the heat and mass transfer in the material together with the desorption of physically adsorbed water and the decomposition of the water of crystallization. The calculated pressure range was in agreements with the previously reported experimental data. By using the model, the sensitivities of permeability, initial water content and the wall thickness were examined. As a result, the maximum pore pressure is very sensitive to permeability, much less sensitive to initial water content and wall thickness. It can be said that the permeability is the controlling factor of the pore pressure rise in cement mortar walls during fire.
KEY WORDS: cement mortar, heat and mass transfer, pore pressure rise, permeability

NOTATIONS

Alphabets		unit	eq.
A^*	pre-exponential factor	[1/s]	(7)
c	specific heat	[J/kg·K]	(1)
D_v	vapor diffusion coefficient	[m^2/s]	(3)
D_w	water diffusion coefficient	[m^2/s]	(4)
E^*	apparent activation energy	[J/kmol]	(7)
L_s	latent heat of desorption	[J/kg]	(1)
L_d	latent heat of decomposition	[J/kg]	(1)
R_{sorp}	rate of desorption	[kg/m^3·s]	(1)
R_{dcmp}	rate of decomposition	[kg/m^3·s]	(1)
T	absolute temperature	[K]	(7)
t	time	[s]	(1)
$\mathbf{u}$	apparent velocity of gas	[m/s]	(2)
w	content of physically adsorbed water	[kg/kg]	(4)
w_{eq}	equilibrium water content	[kg/kg]	(6)
w_c	content of water of crystallization	[kg/kg]	(5)

x	distance from exposed surface	[mm]	X	wall thickness	[mm]

Greek Letters		unit	eq.			unit	eq.
γ	rate constant of desorption	[kg/m^3·s]	(6)	ρ_g	density of gaseous mixture	[kg/m^3]	(2)
ε	void fraction	[m^3/m^3]	(2)	ρ_v	density of water vapor	[kg/m^3]	(3)
θ	temperature	[℃]	(1)	λ	thermal conductivity	[W/m·K]	(1)
ρ_0	dry density of cement mortar	[kg/m^3]	(4)	κ_D	permeability	[m^2/Pa·s]	(8)

Subscripts			
0	dry	ini	initial
k	stage of decomposition	max	maximum

INTRODUCTION

During fire, cement mortar members are intensely heated. Due to the desorption of physically adsorbed water, pore pressure considerably rises. Excessive pore pressure rise may alter the stress field in the material. Spalling might be one of the most significant consequence of it. Therefore the mechanism of pore pressure rise during fire must be clarified in relation with design parameters in order to assure the integrity of concrete and cement mortar during fire.

Concerning with this problem, several experimental studies were carried out so far. Sertmehmetoglu[1] measured the pore pressure of 70 mm concrete wall whose rear surface was sealed and insulated. The measured maximum pressure was about 0.85 MPa (8.5 ata). The authors measured the pressure in a 100 mm concrete slab[2] and 40 mm cement mortar walls[3] at their center. The maximum pore pressure was about 0.3 to 0.4 MPa (3 to 4 ata) for 100mm concrete slabs, 0.12 to 0.24 MPa (1.2 to 2.4 ata) for 40mm cement mortar.

The above measurements are still not enough to correlate the pore pressure with design parameters. It can be said that the pressure rise depends upon permeability, water content and other parameters. In order to derive the relationship between pore pressure and these parameters, analytical approaches such as by Harmathy[4], Huang et al[5], Sahota et al[6] and Dayan et al[7] and the authors[3] are useful. The authors have already presented a comprehensive model of heat and mass transfer that takes into account of desorption and decomposition of water. The model has been verified by comparisons with experimental data for cement mortar walls[3], concrete walls[8], composite floors[9]. In this paper, the model is applied to flat cement mortar walls to investigate the sensitivity of permeability, initial water content and wall thickness.

A MODEL OF HEAT AND MASS TRANSFER[3]

To simulate the heat and mass transfer process, cement mortar is treated as a porous material as shown in figure 1. The conservation equations of heat, gaseous mixture, water vapor, physically adsorbed water and the water of crystallization are

$$\rho c \frac{\partial \theta}{\partial t} = \nabla(\lambda \nabla \theta) - (L_s R_{sorp} + L_d R_{dcmp}), \tag{1}$$

$$\frac{\partial(\varepsilon \rho_g)}{\partial t} + \nabla(\rho_g \mathbf{u}) = R_{sorp} + R_{dcmp}, \tag{2}$$

$$\frac{\partial(\varepsilon \rho_v)}{\partial t} + \nabla(\rho_v \mathbf{u}) = \nabla(D_v \nabla \rho_v) + R_{sorp} + R_{dcmp}, \tag{3}$$

$$\rho_0 \frac{\partial w}{\partial t} = \nabla(\rho_0 D_w \nabla w) - R_{sorp}, \tag{4}$$

$$\rho_0 \frac{\partial w_c}{\partial t} = -R_{dcmp}. \tag{5}$$

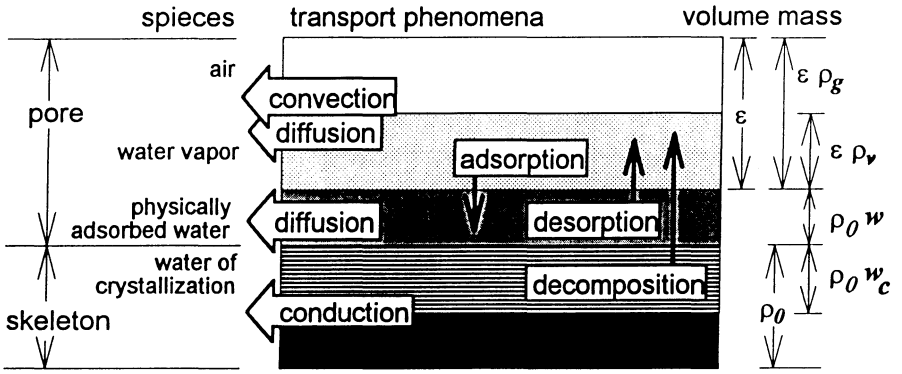

Figure 1 a model of heat and mass transfer

These equations are solved with the rate equations of desorption (Langmuir Equation) and decomposition (Arrhenius Equation)

$$R_{sorp} = \gamma(w - w_{eq}), \tag{6}$$

$$R_{dcmp} = \rho_0 \sum_{k=1}^{3} w_{c,k} A_{d,k} \exp(-E_{d,k} / RT), \tag{7}$$

where in equation (7), subscript $k(=1,2,3)$ denotes the stages of decomposition. In the first stage ($k=1$) the decomposition of gel water takes place at 100 to 300 ℃, At higher temperature calcium hydroxide ($Ca(OH)_2$, $k=2$, at 400 to 450 ℃) and calcium silicate hydrates (CSH, $k=3$, at 600 to 800℃) are decomposed.

In order to close the system, Darcy's equation for gas filtration,

$$\mathbf{u} = -\kappa_D \nabla P_g, \tag{8}$$

and the equations of state for gaseous mixture and water vapor,

$$\rho_g = \{P_v M_v + (P_g - P_v) M_a\} / RT, \quad \rho_v = P_v M_v / RT, \tag{9),(10}$$

are coupled.

The material properties are functions of temperature, pressure and water content, namely,

$$\lambda, \rho, c, \kappa_D, D_v, D_w, \varepsilon = f(\theta, P_g, P_v, w, w_c). \tag{11}$$

These functions are plotted in figure 2, except the permeability κ_D, which will be discussed later.

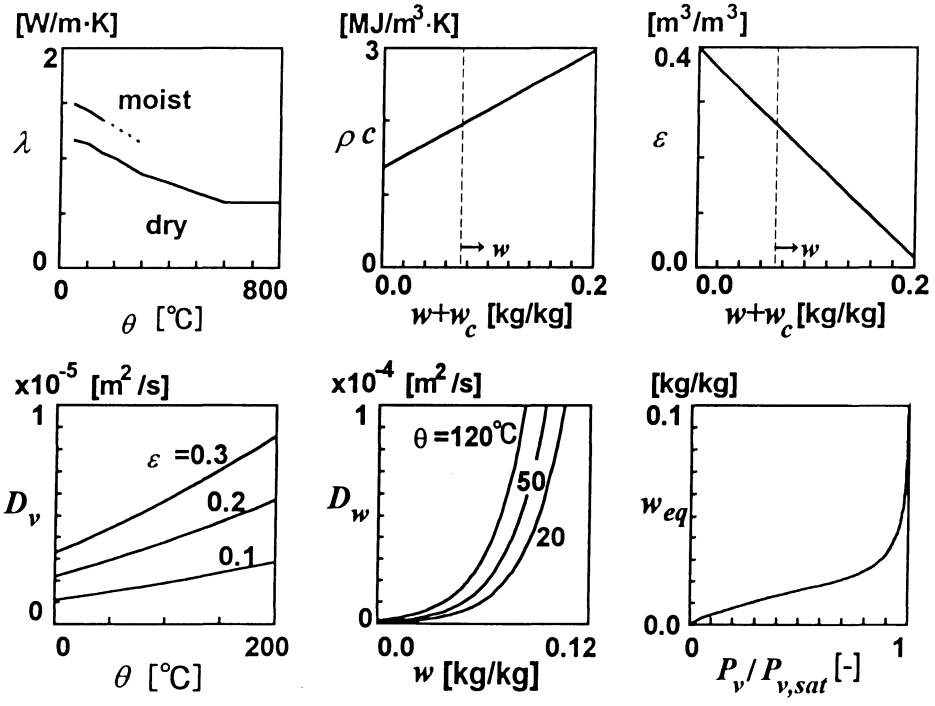

Figure 2 material properties

NUMERICAL METHOD

The governing equations are nonlinear and stiff. In order to overcome numerical instability, they were transformed into integral equations and integrated with respect to time by *S*-stable diagonally implicit Runge-Kutta scheme[10].

The wall was divided by 1mm-thick elements as shown in figure 3. The time increment Δt was 5 seconds, which is very large for the calculation of this kind. The computational time was about three hours by a workstation*.

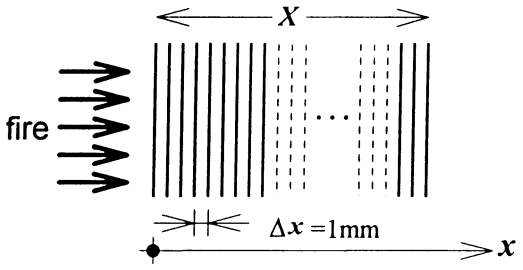

Figure 3 element division

PARAMETERS IN SENSITIVITY ANALYSIS

The wall thickness, permeability and initial water content were selected as parameters in this study. Calculation conditions are summarized in Table 1. The calculations were carried out for all the combinations of these parameters. Total cases were 54.

Table 1 Summary of calculation conditions

parameter	variation	numbers of cases	total
permeability	large, standard, small	3	
initial water content	1,2,3,4,5,6%-wt.	6	$3\times6\times3=54$
wall thickness	40, 60, 80mm	3	

Permeability

Numerous permeability data for concrete and cement mortar were reported in literature. However the reported values are scattered in a wide range as shown in figure 4. Here we assume that the dependence of permeability upon porosity is described by,

$$\kappa_D = c\frac{\varepsilon^3}{(1-\varepsilon)^2} \tag{12}$$

where the coefficient $c(=4.47\times10^{-9})$ was determined so that the correlated curve goes through the center of the data, which will be stated as 'standard' hereafter. The coefficient was multiplied by ten ('large' hereafter) or divided by ten ('small' hereafter).

* MFLOPS=13, SPECint92=36, SPECfp=72

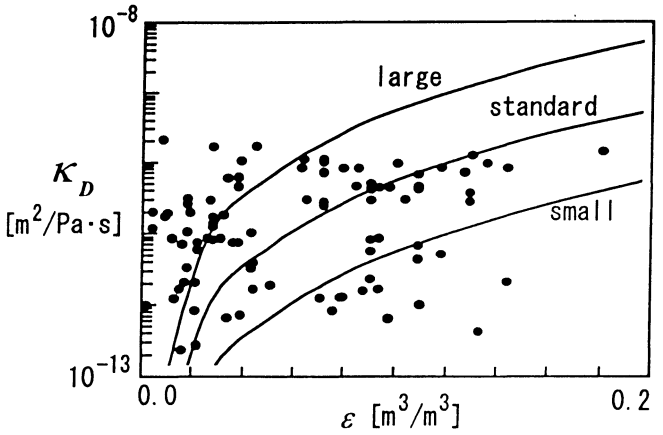

Figure 4 permeability of cement mortar
(filled circles = data from literature[11], solid lines = correlated curves)

Initial Water Content and Wall thickness

The initial water content was varied in the range of 1 to 6% by weight. The wall thickness was changed to 40, 60 and 80mm respectively.

Other Conditions

The slab was assumed to be heated in accordance with ISO 834 standard fire. Initial and ambient temperature was 20℃.

RESULTS

Change of Temperature, Pressure and Moisture Profiles with Time

In figure 5, the profiles of temperature, pressure and water content are shown as functions of time in the case of 40mm thick wall with standard permeability and 3% initial water content. As shown in figure 5a), the temperature at the exposed surface ($x = 0$) rises rapidly. At the positions far from exposed surface, temperature rise is slow. Especially at 30 to 40mm from exposed surface in 15 to 25 minutes, the temperature is kept almost constant due to the desorption of adsorbed water. (so called 'creeping of temperature'). It should be noted that temperature gradient is largest in this time period.

As shown in figures 5b) and 5c), the pore pressures considerably rise up due to the desorption of physically adsorbed water. The total pressure reaches its maximum in 19 minutes at 26mm from the exposed surface. The value is about 0.255 MPa (2.55 ata). At the same time and position, the partial pressure of water vapor reaches its maximum. The value is about 0.231 MPa (2.31 ata). The difference of the two maximum values is about 0.024 MPa (0.24 ata), which means that about quarter of the air is still trapped in the pore.

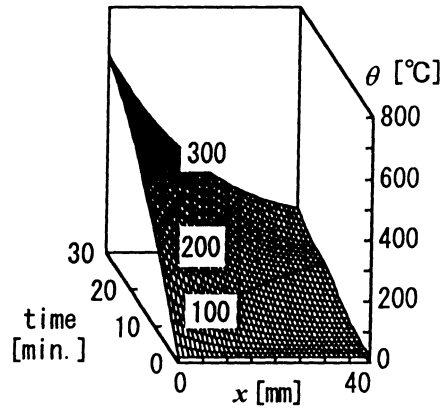

a) temperature

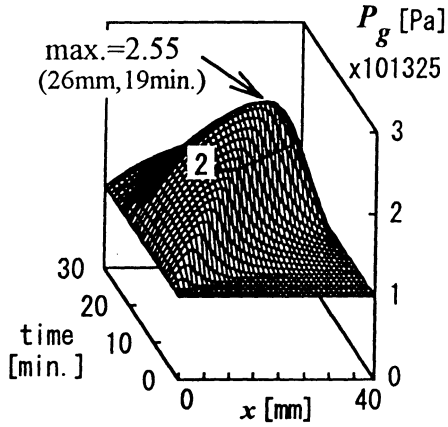

b) total pressure

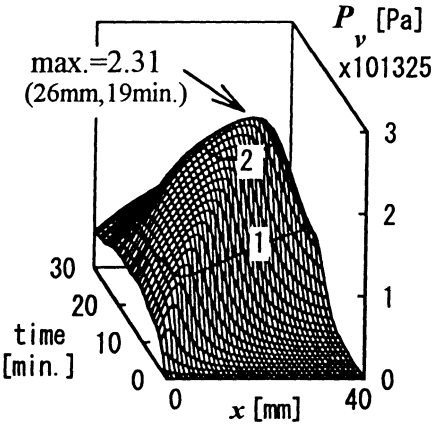

c) vapor pressure

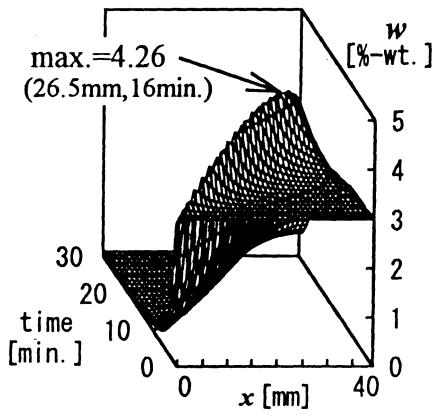

d) physically adsorbed water

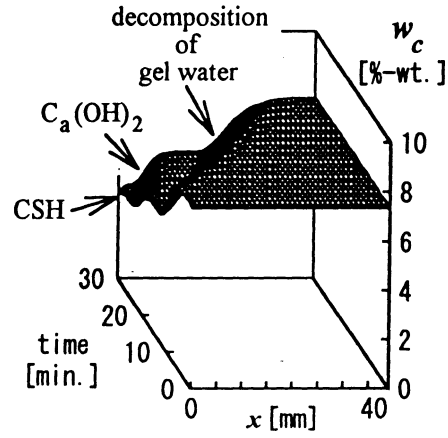

e) water of crystallization

Figure 5 calculated results for κ_D= standard, w_{ini}=3%-wt., L= 40mm

In figure 5d), the profile of physically adsorbed water is shown. At all the positions except for the exposed surface, water content rises due to the adsorption of water vapor. After reaching to a certain value, it falls down due to the desorption. The maximum water content occurs in 16 minutes at 26.5mm from the exposed surface. By comparing with that for total and vapor pressures, the position is almost the same, however the time is slightly earlier.

In figure 5e), the profile of water of crystallization is shown. The water of crystallization decomposes in three stages after the physically adsorbed water was lost.

The Effect of Permeability

To analyze the effect of permeability, the results for 40mm thick wall with 3% initial water content are analyzed. In figure 6, the temperature, pressure and water content profile when the temperature at exposed surface reached 400℃ is plotted in the cases of large, standard and small permeability. In the temperature profile shown in figure 6a), difference can be seen in the temperature range of 110 to 160℃ . As the permeability is increased, the desorption temperature approaches to 100℃. As a result, temperature gradient is increased. This is in accordance with the water content profile in figure 6c).

As shown in figure 6b), the pore pressure is greatly influenced by permeability. In case of large permeability, the pore pressure rise is quite small. The value of total pressure is almost equal to that of vapor pressure, which means that most of the air has been already pushed out from the pore. In case of small permeability, the total pressure rises as much as 0.52MPa (5.2 ata). It can be also pointed out that there is a considerable difference between total and vapor pressures, which means that a large amount of air is still trapped in the pore.

The Effect of Initial Water Content

In figure 7, the results for 40mm thick wall with standard permeability are shown in a similar way with figure 6, varying the initial water content. As shown in figure 7a), the temperature profile is greatly influenced by the initial water content. Especially in the cases of 1 to 4% of initial water content. However the profiles for 4 to 6% are almost identical. The effect of initial water content upon temperature profile is limited to a certain degree.

Similar tendency exists in the pressure (figure 7b) and water content (figure 7b) profiles. In the pressure profile, there are no significant changes even if the initial water content is increased to more than 3%. In the water content profile, it can be seen that the location of drying front is not influenced if the initial water content is more than 4%. One of the reasons for this tendency is that the rate of desorption is limited by the rate of heat supply to the drying front.

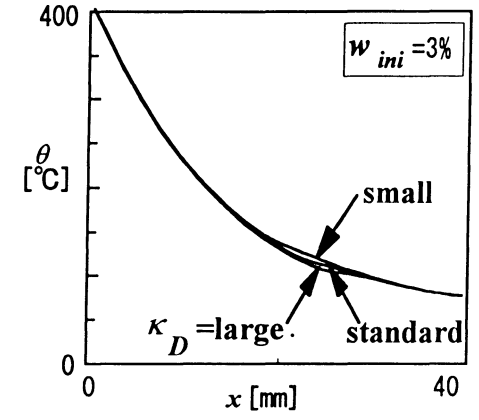

a) temperature profile

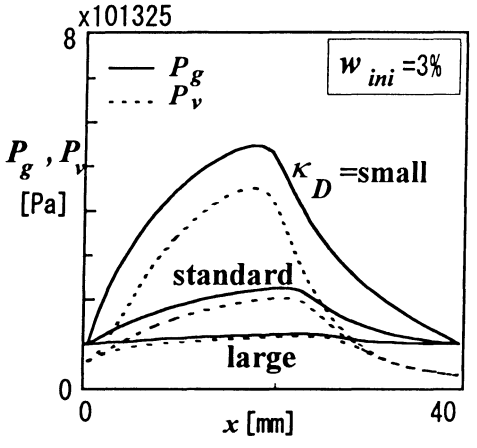

b) pressure profile

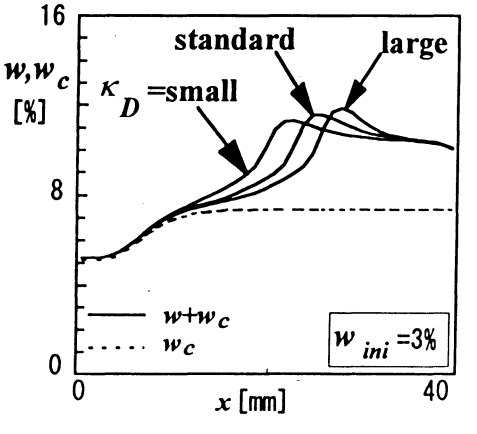

c) water content profile

Figure 6 effect of permeability upon temperature, pressure and water content profiles

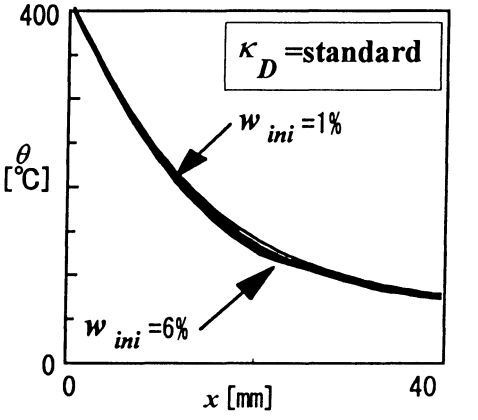

a) temperature profile

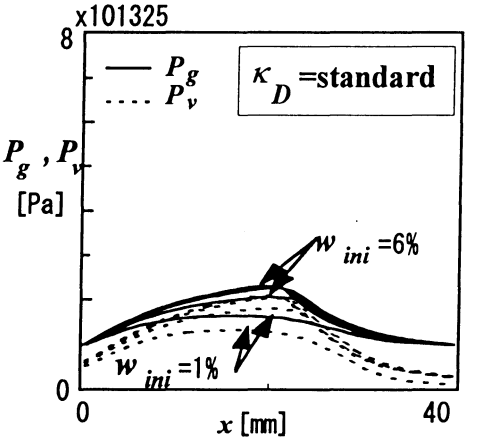

b) pressure profile

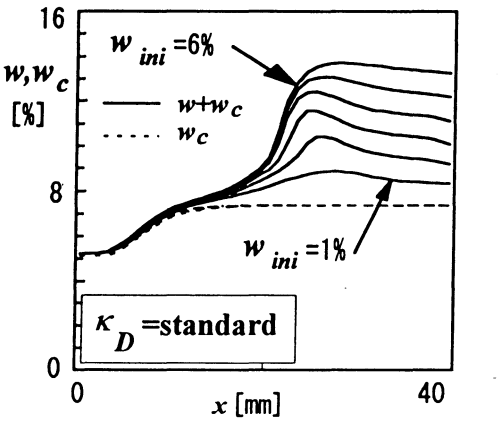

c) water content profile

Figure 7 effect of initial water content upon temperature, pressure and water content profiles

Maximum Pore Pressure

The maximum pore pressure for 40mm thick wall is shown in figure 8. As was described above, the maximum pore pressure is strongly dependent upon the permeability, weakly dependent upon the initial water content. The same tendency exists in this figure. In case of small permeability, maximum pressure changes from 0.48 MPa (4.8 ata) to 0.68 MPa (6.8 ata) as the initial water content changes from 1 to 3 %-wt. However there are almost no more changes even if the initial water content is further increased. The same tendency exists in the cases of standard and large permeability.

The previously reported experimental data[3] is also plotted in figure 8. The experiments were carried out for three times. In the experiments No. 1 and No. 3, visible cracks were observed. Thus the pore pressure rise was not so significant. In the experiment No. 2, there were no visible cracks. Thus the pressure rose up to 0.24 MPa (2.4 ata). The corresponding permeability values in experiments fall between 'standard' and 'large' values. Even though the permeability strictly depends on the degree of crack formation, it would be adequate to use 'standard' value in order to calculate the maximum pore pressure rise conservatively.

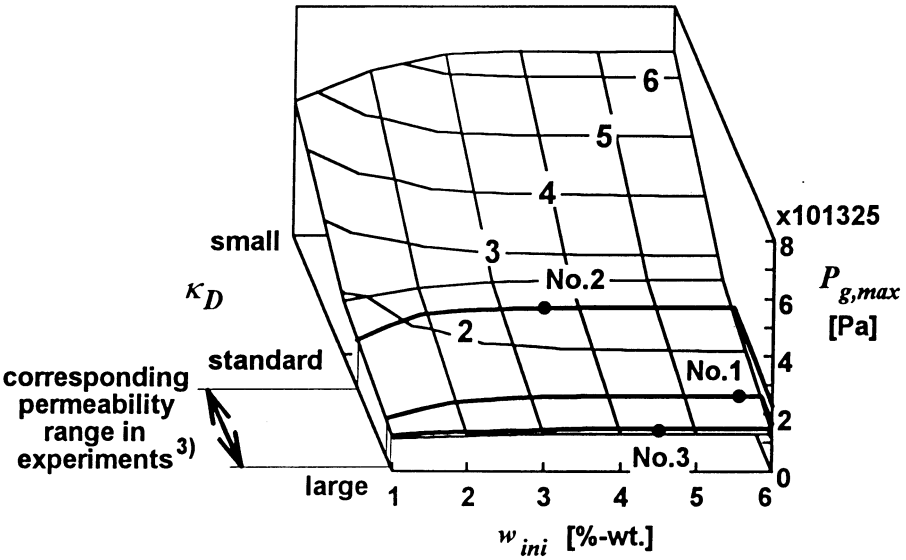

Figure 8 the effect of permeability and initial water content upon maximum pore pressure contours = calculated results, filled circles = experimental data[3]

The Effect of Wall Thickness upon Pore Pressure

In figure 9, maximum pore pressure is plotted versus the wall thickness. As can be seen from this figure, the effect of wall thickness is not so significant. Even in the case of small permeability and 6% initial water content, the increase in the maximum pressure is about 15% when the wall thickness is increased from 40 to 80 mm. There is almost no effect in case of large permeability and 1% initial water content.

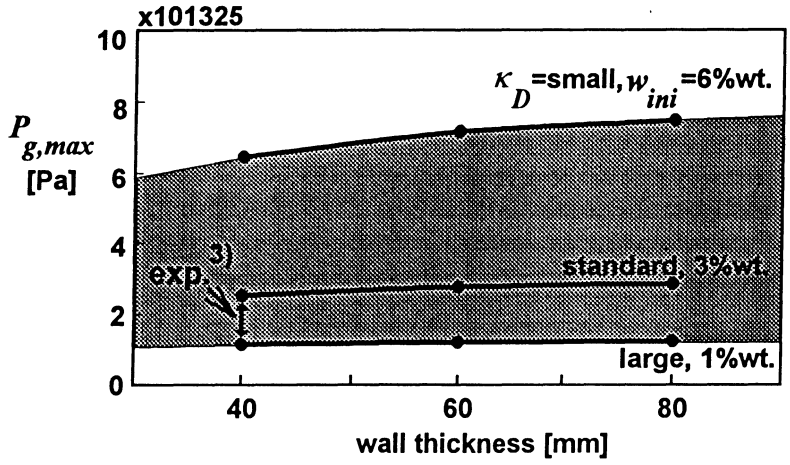

Figure 9 the effect of wall thickness upon maximum pore pressure
(hatched area = range of calculated values, exp. = range of experimental data[3])

COMMENTS ON SPALLING

Occasionally concrete elements are destroyed by spalling. One of the reasons for spalling is the development of thermal stress due to temperature change. A theory to describe the mechanism of spalling was presented by Saito[12]. In the theory, the main cause of destructive spalling of prestressed concrete is the compressive failure at the exposed surface. Following his theory, the temperature profile should be predicted as accurately as possible in order to evaluate the possibility of destructive spalling. In this sense, the approach in this study is useful because the effect of design parameters upon temperature profile can be analyzed as was done in figures 6 and 7.

Even though the main reason for spalling is the development of thermal stress, the development of pore pressure may contribute to spalling. Conventional structural concrete has at least more than 15 MPa (150 ata) of compressive strength and 1.5 MPa (15 ata) of tensile strength. The maximum pore pressure calculated in this study is far below the compressive strength, but comparable with tensile strength. Therefore the development of pore pressure may alter the stress field in the material.

CONCLUSIONS

The pore pressure in cement mortar walls under ISO834 fire was calculated by using a model of heat and mass transfer. The sensitivities of permeability, initial water content and wall thickness were analyzed. The calculated pressure range covered the previously reported experimental data. Thus the calculated results would be adequate.

The sensitivities of above parameters upon temperature, pressure and water content profiles were analyzed. Among the three, the permeability is the dominating one. The rest two are less

significant. As the initial water content is increased, the maximum pore pressure is increased only to a certain limit. As the wall thickness is increased, the pore pressure is slightly increased only when the permeability is small.

ACKNOWLEDGMENTS

Part of this study was financially supported by a Grant-in-Aid for Scientific Research from the Ministry of Education of Japan.

REFERENCES

1. Sertmehmetoglu, Y., On a mechanism of spalling of Concrete under fire conditions, Ph.D. thesis, University of London, 1977 (reviewed by Dougill, J., W., Materials Dominated Aspects of Design for Structural Fire Resistance of Concrete Structures, ACI SP80-4, pp. 151-175, American Concrete Institute, 1983)
2. Terai, T., Shohouin, Y., Fujikawa, S, Mitamura, S. ,Yoshida, M., Tasaka, S., Harada, K., "A Study on Temperature History in Concrete of Composite Floor in Fire", Summaries of Annual Meeting, Series A, Architectural Institute of Japan, pp. 761-766, (in Japanese), 1987
3. Harada, K., Terai, T., "Heat and Mass Transfer in an Intensely Heated Mortar Wall", Fire Safety Science, 3, pp. 781-790, Elsevier Applied Science, 1991
4. Harmathy, T., Z., "Simultaneous Moisture and Heat Transfer in Porous Systems with Particular Reference to Drying", Ind. Eng. Chem., 8, pp. 92-103, 1969
5. Huang, C., L., D., Siang, H., H., Best, C., H., "Heat and Moisture Transfer in Concrete Slabs", Int. J. on Heat and Mass Transfer, 22, pp. 257-266, 1979
6. Sahota, M., S., Pagni, P., J., "Heat and Mass Transfer in Porous Media Subjected to Fires", Int. J. on Heat and Mass Transfer, 22, pp. 1069-1081, 1979
7. Dayan, A., Gluekeler, E., L., "Heat and Mass Transfer within an Intensely Heated Concrete Slab", Int. J. on Heat and Mass Transfer, 25(10), pp. 1461-1467, 1982
8. Harada, K., Terai, T., "Fire Resistance of Concrete Walls", Fire Science and Technology, pp. 215-220, International Academic Publishers, 1992
9. Harada, K., Terai, T., "Dependence of Thermal Responses of Composite Slabs Subjected to Fire on Cross sectional Shapes", Fire Safety Science, 4, pp. 1159- 1170, Elsevier Applied Science, 1994
10. Terai, T., Harada, K., "Fire Behavior of Concrete Members Taking into account Simultaneous Transfer of Heat and Moisture", '93 Asian Fire Seminar, 1993
11. data from 14 papers by Murata, J., Hayashi et. al., Langley, A., A., Cabera, J., G., Hanaor, A., et al., Saito, T., et al., Tamai, M., et al., Yokomichi, H., et al., Nyame, B., K., Vuorien, J., Watson, A., J. (Reviewed by Harada, K., in A Study of Predicting the Temperature Rise of Concrete During Fire Resistance Test (in Japanese), Doctoral Dissertation, Kyoto University, 1994)
12. Saito, H., "Explosive Spalling of Prestressed Concrete in Fire", Bulletin of Fire Prevention Society of Japan (in Japanese), 15(2), pp. 23- 30, 1966